JOURNAL OF PROPULSION AND POWER
Vol. 11, No. 3, May–June 1995

# Vortex Generation and Mixing in Three-Dimensional Supersonic Combustors

D. W. Riggins*
*University of Missouri–Rolla, Rolla, Missouri 65401*
and
P. H. Vitt†
*Analytical Services and Materials, Inc., Hampton, Virginia 23681*

**The generation and evolution of the flow vorticity established by instream injector ramps in a high Mach number/high enthalpy scramjet combustor flowfield are described in detail for a number of computational cases. Classical fluid dynamic circulation is presented for these cases in order to clarify the spatial distribution and convection of the vorticity. The ability of the simulations to accurately represent Stokes law of circulation is discussed and shown. In addition, the conservation of swirl is presented for these flows. The impact of both turbulent diffusion and the vortex/ramp nonuniformity on the downstream mixing rate is clearly illustrated. A correlation over the length of the combustor between fuel-air mixing and a parameter called the vortex stirring length is demonstrated. Finally, computational results for a representative ramp injector are compared with experimental data.**

## Nomenclature

$\mathbf{dl}$ = differential line element (vector)
$L_{vs}$ = vortex stirring length
$\boldsymbol{n}$ = unit normal vector from surface $S$
$\boldsymbol{q}$ = velocity vector
$\boldsymbol{r}$ = position vector
$T$ = torque
$\Gamma$ = circulation
$\rho$ = fluid density
$\Phi$ = fuel equivalence ratio
$\boldsymbol{\omega}$ = vorticity vector
$\boldsymbol{\omega}_x$ = axial (downstream) component of vorticity vector

## Introduction

THE successful development of air-breathing scramjet engines for hypersonic aircraft requires the innovative design of three-dimensional combustors such that when fuel is injected, mixing and burning occur as rapidly as possible with minimal flow losses.[1] Numerous two-dimensional shear layer studies have shown slow mixing for high Mach number flows. However, past experimental and computational investigations for three-dimensional scramjet combustor flowfields have demonstrated that relatively fast mixing can be established by the generation of flow vortices from either fuel injector ramps or from flush wall injectors.[2] The basic premise of this design technique is that three-dimensional vortices generated and shed by ramps or jets entrain fuel and air and eventually stretch the fuel-air interface such that true (microscale) mixing is significantly increased. The counter-rotating axially directed vortices that are shed from injector ramps are primarily spillage-induced due to pressurization on the ramp face behind the ramp bow shock. Similar vortices associated with flush-wall jets are more complex in their generation; flow features contributing to these vortices include spillage (pressurization on the top of the jet plume behind the injector bow shock) as well as jet shear and momentum effects. These axial vortices, whether generated by ramps or wall jets, can form the most productive downstream mixing component of the overall large-scale vorticity. It should be emphasized, however, that large-scale vortices are only one of many highly coupled flow components that can contribute to fuel-air mixing. Other features that directly relate to mixing include fuel-air velocity ratio, jet pressure ratio, fuel equivalence ratio, and the baroclinic effect of a shock passing through the jet plume.[3] The purpose of the present work is as follows:

1) Provide a basic study of the generation and development of vortices shed from injector ramps in high-enthalpy flows.

2) Investigate the ability of large-scale three-dimensional numerical simulations to accurately represent basic laws associated with these vortices for complex geometries.

3) Investigate the actual influence of the vortices on downstream fuel-air mixing.

4) Compare the numerically predicted flowfield with available experimental data for a representative configuration at high flight Mach number.

The use of ramp vortex generators for enhancing fuel-air mixing has been studied in the past by a number of investigators. Povinelli[4] first examined the injection of helium into the vortex generated by the leading edge of a highly swept delta wing. It was found that the mixing improved with increasing angle of attack of the wing, corresponding to the strength of the generated vortex. A subsequent study by Hersch and Povinelli[5] used a configuration that injected at the confluence of two counter-rotating vortices. These vortices were generated by converging delta wings mounted in the flow ahead of the injector. Swithenbank[6] used the first swept ramp injector in order to investigate the mixing enhancement of ramp generated vorticity. The swept ramp similar to that shown in Fig. 1 generated a 30% increase in wall pressure over the pressure rise for a plain wedge with the same flow blockage in a reacting experiment.

Computational studies[7] of both swept and unswept ramps for a freestream Mach number of 2 showed that the swept ramp generated a stronger bow shock than the unswept ramp. This bow shock generated higher pressures on top of the ramp such that stronger vortices were shed from the sides of the

Presented as Paper 93-2144 at the AIAA/SAE/ASME/ASEE 29th Joint Propulsion Conference and Exhibit, Monterey, CA, June 28–30, 1993; received July 27, 1993; revision received Aug. 31, 1994; accepted for publication Sept. 14, 1994. 

*Assistant Professor, Department of Mechanical and Aerospace Engineering. Member AIAA.
†Research Engineer. Member AIAA.

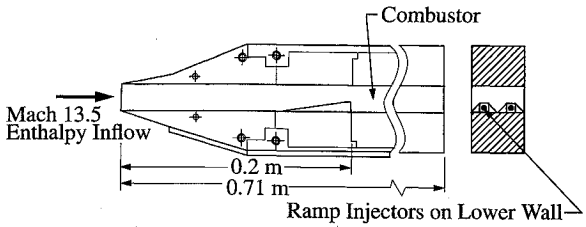


**Fig. 1 Schematic of swept ramp injectors and duct.**

ramp. The vortices interacted with the fuel jet causing the fuel-air interface to stretch, hence, increasing the mixing. Riggins[8] also analyzed the flow losses associated with increased mixing by examining various injection strategies for the same freestream Mach number. Several subsequent experimental and computational studies[1,9] have examined ramp and wall jet configurations for high enthalpy flows. Techniques have been developed to study the actual thrust potential of various injection strategies.[1]

In order to further study the highly three-dimensional vortices generated by ramp injectors at high enthalpies (corresponding to a vehicle flight Mach number of 13.5), a series of computational cases is analyzed in this article. For this study, a baseline swept ramp injector similar to those tested in the HYPULSE facility[10] is defined. The flow over this injector is modeled using both inviscid and laminar flow for two grid levels. Fuel is injected from the ramp base with velocity approximately matched to freestream velocity such that fuel-air velocity ratio effects on mixing are minimized. Vortices generated by either flush-wall jets or intrusive injectors can be represented mathematically by the classical fluid circulation on a cross-sectional plane of a combustor. Therefore, in order to gain confidence in the ability of the simulation to accurately model the vorticity generation in such geometries, Stokes law of circulation is presented for relevant solutions. A fundamental check of the conservation of angular momentum (i.e., the equality of the torque on the combustor with the change in flow moment-of-momentum) is also described and is presented for both inviscid and viscous cases. Fuel-air mixing is compared between the baseline swept ramp case and a straight-sided (unswept) ramp case. The concept of the vortex stirring length is shown to correlate the mixing in both cases. The impact of the vorticity (and other ramp-induced nonuniformities including the bow shock and the ramp shear layer) on downstream mixing is further studied by comparing the mixing obtained from two turbulent cases; one of which essentially eliminates the nonuniformity (including the ramp vortex) at the ramp base by suitably one dimensionalizing the flow at that point. Finally, a swept ramp in an actual HYPULSE configuration is described and a comparison of computed wall pressure vs experimental data is made.

## Fluid Theorems

This section briefly describes fundamental laws that will be applied to CFD solutions in the results section. Two basic theorems are introduced: 1) Stokes circulation law and 2) moment-of-momentum.

### Stokes Theorem

In this work, the ability of the simulations to satisfy the fundamental Stokes law is presented for a number of injector ramp cases. Stokes theorem relates the fluid dynamic circulation as computed using the surface integrated vorticity to the line integral of the velocity taken around the surface of interest, i.e.,

$$\Gamma = \int_s \boldsymbol{\omega}\cdot\boldsymbol{n}\,\mathrm{d}S = \int_c \boldsymbol{q}\cdot\mathrm{d}\boldsymbol{l} \qquad (1)$$

For the purpose of this work, the circulation is defined to be the value associated with a given crossflow plane, i.e., associated particularly with $\omega_x$. Note that Stokes theorem (1) is valid for any steady inviscid or viscous flow. This theorem provides a fundamental criteria that should be examined in numerical simulations of three-dimensional vortex-enhanced combustor flowfields. Note that the net circulation would be zero on an entire ramp due to the symmetric counter-rotating vortex pair.

### Conservation of Angular Momentum

A basic conservation principle for three-dimensional scramjet combustor flows is the conservation of swirl (or moment-of-momentum). This theorem (for steady flow) states that the change in angular momentum of the flow in a control volume must be equal to the net torque exerted on the control surface, or

$$\sum \boldsymbol{T} = \int_s \rho(\boldsymbol{r}\times\boldsymbol{q})(\boldsymbol{q}\cdot\boldsymbol{n})\,\mathrm{d}S \qquad (2)$$

$S$ is taken as the confined cross-sectional area of the combustor, or more precisely, the computational domain as described in subsequent sections. The torques acting on the boundaries are moments due to pressure forces and viscous stresses. The origin in this work is the upper left point of the computational domain looking upstream towards the base of the ramp. Integration for both moment-of-momentum and circulation is performed by summing components in individual computational cells on the cross-sectional plane of interest. The torque and moment-of-momentum are referenced to the cross-sectional plane at the leading edge of the ramp.

## Description of Codes

The fourth-order accurate SPARK family of Navier-Stokes codes,[11-14] which includes a three-dimensional elliptic version and a parabolized (PNS) version is used in this work. For this work, a modified algebraic model[1] is used for several cases in order to generate the turbulent viscosity downstream of ramps. This model is practical from a resource standpoint and has been successfully applied for engineering mixing predictions in low-enthalpy injector flows. It should be emphasized that this model, as modified and used in these and other studies, only represents a qualitative modeling technique used to predict downstream mixing and mean-flow. Details of the highly complex turbulent viscosity distribution are not accurately predicted by this model. For the prediction of turbulent diffusion of mass, an effective Schmidt number of 0.5 is used for all calculations.

## Case Summary

This section briefly reviews the order and rationale for all cases presented in this work (see Table 1). Further details concerning geometry, grids, and boundary conditions are given in subsequent sections.

Case a–g in Table 1 are defined in order to analyze vortex generation, evolution, mixing, and conservation theorems associated with swirl and vorticity. Case a is a fine grid inviscid solution and case b is a coarse grid inviscid solution for a swept injector ramp with axial injection from the base. Case c is a laminar solution and case d is a turbulent solution for the same geometry and flow conditions as cases a and b. This allows a comparative study of the influence of viscosity on vortex generation and downstream macromixing. Case e is the same as case d, except that a straight-sided (unswept) ramp is modeled. Cases f and g replace the discrete hydrogen orifice in the base of the ramp used in cases a–e with hydrogen injection from the entire base while maintaining the same fuel equivalence ratio (the injection pressure is lowered). Although both of these cases use turbulence modeling, case g one dimensionalizes the flow at the ramp base in order to study the ramp vortex impact on mixing.

**Table 1 Case summary**

| Case[a] | Elliptic grid (half-ramp) | Φ | Flow type | Jet conditions |
|---|---|---|---|---|
| a | 101 × 81 × 61 | 1.0 | Air-inviscid | $U$ = 3,385 m/s<br>$P$ = 97,528 N/m$^2$<br>$T$ = 704 K |
| b | 51 × 41 × 31 | 1.0 | Air-inviscid | $U$ = 3,385 m/s<br>$P$ = 97,528 N/m$^2$<br>$T$ = 704 K |
| c | 101 × 81 × 61 | 1.0 | Air-laminar | $U$ = 3,385 m/s<br>$P$ = 97,528 N/m$^2$<br>$T$ = 704 K |
| d | 101 × 81 × 61 | 1.0 | Air-laminar (ramp)<br>Turbulent (downstream) | $U$ = 3,385 m/s<br>$P$ = 97,528 N/m$^2$<br>$T$ = 704 K |
| e | 101 × 81 × 61 (unswept) | 1.0 | Air-laminar (ramp)<br>Turbulent (downstream) | $U$ = 3,385 m/s<br>$P$ = 97,528 N/m$^2$<br>$T$ = 704 K |
| f | 101 × 81 × 61 | 1.0 | Air-laminar (ramp)<br>Turbulent (downstream) | $U$ = 3,385 m/s<br>$P$ = 22,351 N/m$^2$<br>$T$ = 704 K (fill base) |
| g | 101 × 81 × 61 | 1.0 | Air-laminar (ramp)<br>Turbulent (downstream)<br>(vortex removed) | $U$ = 3,385 m/s<br>$P$ = 22,351 N/m$^2$<br>$T$ = 704 K (fill base) |
| h[b] | 81 × 61 × 61 (entire ramp) | 1.0 | $N_2$-laminar (ramp)<br>Turbulent (downstream)<br>$Pr_T$ = 0.5<br>($Le_T$ = 1.0) | $U$ = 3,249 m/s<br>$P$ = 224,697 N/m$^2$<br>$T$ = 1,159 K<br>$\alpha_{H_2}$ = 0.543<br>$\alpha_{H_2O}$ = 0.4573 |

[a]All cases used inflow with $U$ = 3840 m/s, $P$ = 18,197 N/m$^2$, and $T$ = 2350 K; jet to freestream velocity ratio ~ 1.0 for all cases/swept ramp unless otherwise noted.
[b]Actual HYPULSE duct (sidewall and upstream duct).

Finally, case h is a CFD simulation of a mixing experiment performed in the HYPULSE combustor duct. This simulation includes a nonuniform inflow for the swept ramp section as well as side walls and a complex injectant. A direct comparison with experimental data is provided for this case.

## Grids and Boundary Conditions

All cases summarized in Table 1 are based on ramp injector geometries similar to those shown schematically in Fig. 1.

The ramps for computational cases a–g are modeled using a slanted Cartesian grid approach described in an earlier work.[2] The ramps have 10.3-deg top compression surfaces with sides swept back at 10 deg, except for case e, which is unswept. They are approximately 4 cm long. The injector orifice is sized for cases a–e using an injectant Mach number of 1.7 and a fuel equivalence ratio of 1.0. The constant area combustor length from the ramp leading edge is approximately 60 cm. Further details of the duct and ramp geometries can be obtained in Refs. 1 and 9. Grids used in the near-field elliptic region for this study (for cases a–g) include a baseline fine grid (101 axial nodes, 81 vertical, and 61 transverse) as well as a coarse grid (51 × 41 × 31) in which every other grid line in the fine grid is deleted. Grids are clustered at all solid walls and at the jet centerline symmetry plane.

Cases a–g have uniform air inflow with axial inflow $U$ velocity of 3840 m/s, temperature of 2350 K, and pressure of 18,197 Pa. Hydrogen fuel conditions for these cases (except as noted below) are $U$ = 3385 m/s, $T$ = 704 K, and pressure $P$ = 97,528 Pa. The fuel jet is angled up at 10.3 deg (parallel to the top surface of the ramp). Fuel equivalence ratio in all cases is 1.0. Cases f and g use a jet pressure of 22,351 Pa and expand the injection orifice area to cover the ramp base (such that the same fuel equivalence ratio of 1.0 is maintained). Cases a–g use symmetry boundary conditions at ramp/injection centerline and the ramp side (i.e., no side wall is present such that only one-half of the ramp is simulated). Wall temperatures are treated adiabatically for these cases. Wall velocity boundary conditions (on top and bottom) are flow tangency for inviscid cases and no-slip for viscous cases.

Case h, which models actual HYPULSE geometry and conditions, includes approximately 16 cm of duct upstream of the ramp and a side wall such that the inflow to the elliptic region is highly nonuniform. Wall temperatures are fixed at 300 K for this case. The grid in the near-field is 81 × 61 × 61. In this case, the fuel included a hot seed required by the experimental instrumentation (see Table 1).

## Computational Approach

The computational strategy that is utilized in this study has been fully described in previous references.[1,2] The upstream region (relevant for case h only) is simulated using the three-dimensional PNS code. A fixed inflow is then passed to the three-dimensional elliptic code at the ramp leading edge. The elliptic code encompasses both the ramp (approximately 4 cm long) and the downstream region (to 11 cm beyond the ramp leading edge or 7 cm beyond the base for cases a–g). When this near-field injector region converges to a satisfactory tolerance (see below) the outflow plane from this solution is then passed to the PNS code for downstream marching calculations. For case h, the outflow plane from the elliptic region is passed to the PNS code at approximately one ramp length beyond the ramp base. The strategy of solving the near field using the elliptic code and then passing to the parabolized solver further downstream has been very successful in the past at generating accurate engineering simulations of complex scramjet combustor flowfields.

The ramp section (and the upstream duct for case h) is treated using laminar flow for all cases except cases a and b, which are entirely inviscid. In those comparative cases (d, e, f, g, and h) in which turbulence modeling is used, turbulence is tripped on the bottom wall at the ramp base and on the top wall where the shock reflects from the wall.

Solution convergence in the elliptic near field is defined by a matrix of criteria that includes unchanging mean values of wall pressures and mixing efficiencies as well as mass flow conservation (both fuel and air). Overall mass flow conservation at the elliptic region exit is monitored to ensure a level of less than 1% conservation error.

## Results and Discussion

This section presents the results of the current study for high enthalpy flows. Configurations examined include inviscid and viscous cases with fine and coarse grids. Pressure contours on a longitudinal plane are plotted along the ramp (jet) centerline for the 101 × 81 × 61 inviscid case (case a) and for the laminar case (case c) (Fig. 2). The bow shock from the ramp injector is the dominant feature of the flow. This bow shock is a highly three-dimensional structure due to the three-dimensional relieving over the ramp. It is responsible for the pressure-induced spillage that generates the strong axially directed vortex. The effect of the three-dimensional relieving can be clearly seen by plotting cumulative ramp face pressure drag vs $x$ for a similar case (Fig. 3). Note the relieving along the ramp evident in this figure. The bow shock reflects from the top wall of the combustor duct and intersects the jet plume downstream of the ramp. Vorticity generation can also take place due to the intersection of the shock with the fuel plume. The details of the injection flowfield behind the ramp can be seen in Fig. 2. The effects of viscosity on the pressure contours are minimal for the case shown.

Hydrogen fuel mass fraction contours (Fig. 4) on crossflow planes located 6 cm downstream of the ramp base for the laminar case c show that the fuel jet is highly distorted and warped by the vortex shed from the ramp. This distortion should enhance mixing by effectively stretching the fuel-air interface such that microscale mixing takes place. Since the fuel-air velocity ratio is closely matched (see Table 1), mixing is dominated by laminar and numerical diffusion as well as any base flow effects. The axially directed vorticity shed from the ramp is depicted in Fig. 5, which shows crossflow velocity vectors (case a) at a crossflow plane at the ramp base. Since the computational domain was modeled using a symmetry plane at the ramp injector centerline (half-ramp), only one vortex is seen. This is the left vortex of a counter-rotating pair shed from each ramp in the combustor.

Figure 6 is a plot of circulation strength $\Gamma$ vs axial distance measured from the ramp injector leading edge for both an inviscid fine grid case (case a) and an inviscid coarse grid case (case b). Circulation strength as computed by both integrated vorticity and velocity line integral (providing a Stokes theorem check) is shown. Overall, the circulation strength is seen to increase approximately linearly over the ramp length to the ramp base (at 4 cm), where it reaches a maximum of about 12. The circulation for the fine grid case then drops quickly to about 50% of its ramp maximum value in the ramp base region, then climbs to around 12 again by the end of the elliptic region (at 11 cm). Noting the physical meaning of the circulation (i.e., essentially the rotation of the fluid in the crossflow plane), it is seen that the axial vortex forms and strengthens over the ramp. This vortex is shed from the ramp base and is deflected from the axial direction by ramp base effects

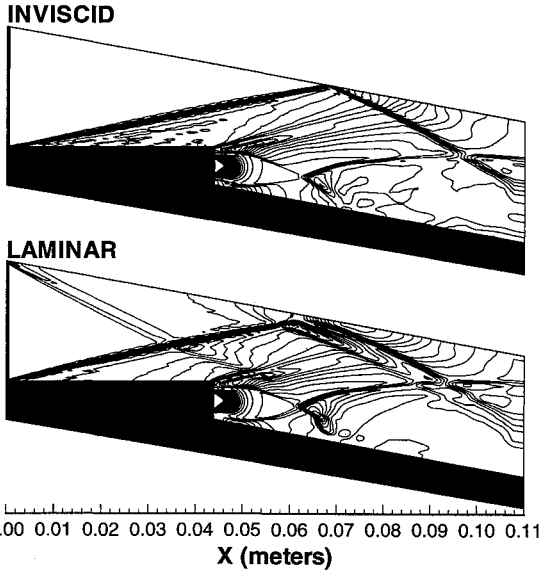


**Fig. 2 Pressure contours on ramp centerline (top-inviscid, bottom-laminar), $P$(max) = 96396 N/m², $P$(min) = 3213 N/m², $\Delta P$ = 3213 N/m².**

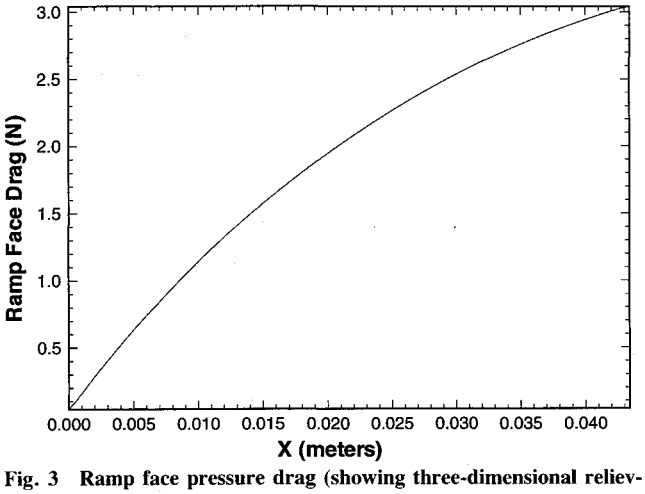


**Fig. 3 Ramp face pressure drag (showing three-dimensional relieving).**

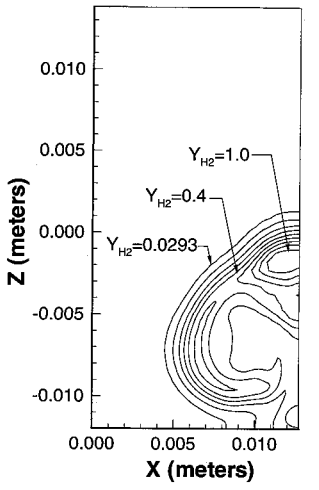


**Fig. 4 Hydrogen mass fraction contours on crossflow plane located 11 cm aft of ramp leading edge.**

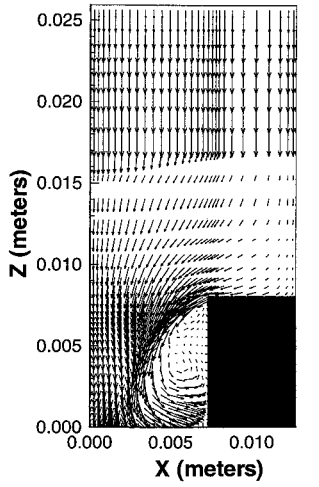


**Fig. 5 Cross-flow plane velocity vectors at ramp base.**

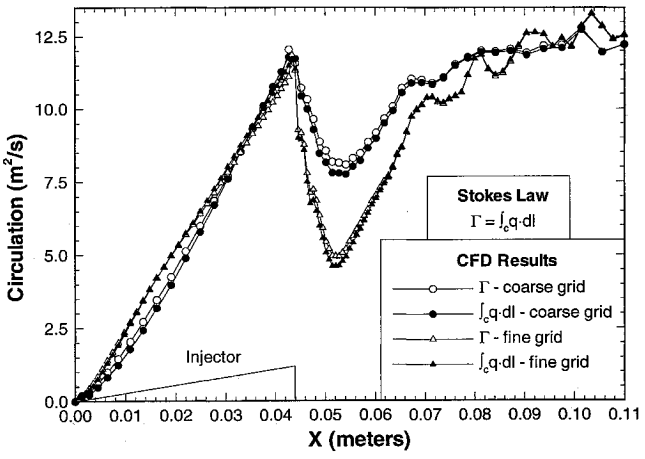


Fig. 6 Circulation (vorticity and line integrals) vs $x$ (inviscid flow).

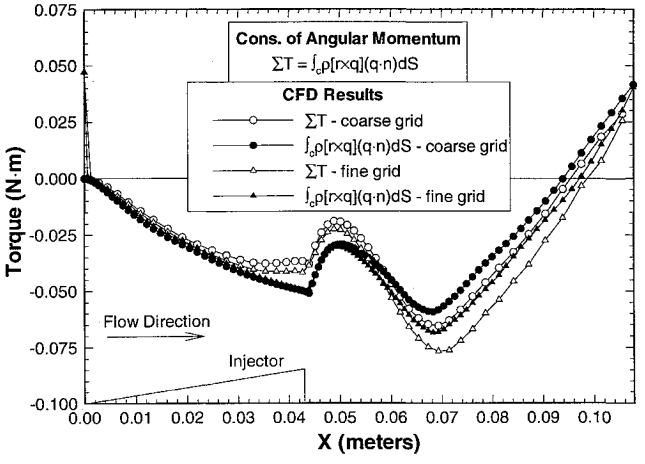


Fig. 7 Torque and moment-of-momentum vs $x$ (inviscid flow).

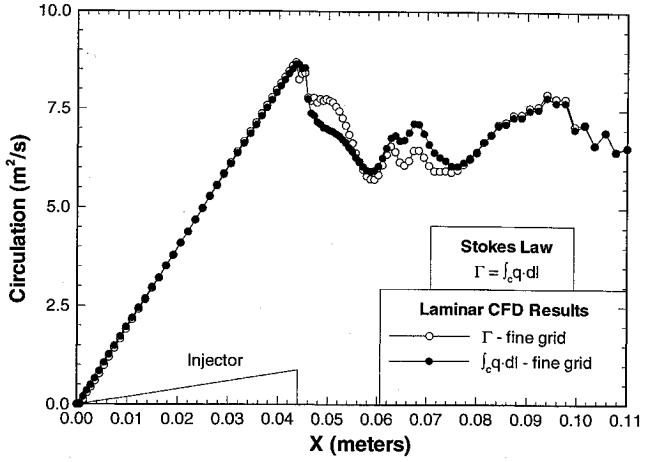


Fig. 8 Circulation (vorticity and line integrals) vs $x$ (laminar flow).

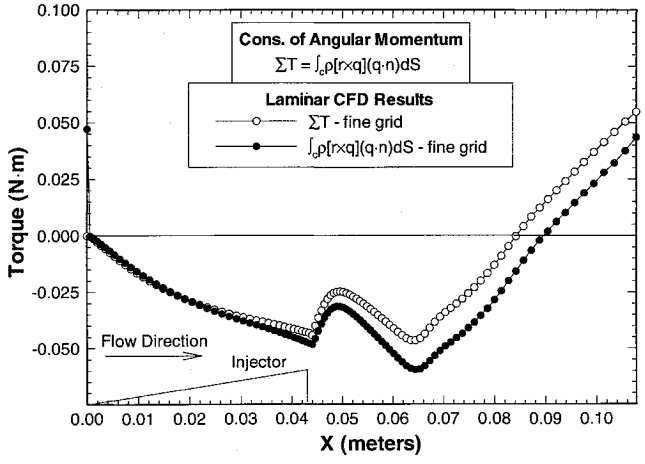


Fig. 9 Torque and moment-of-momentum vs $x$ (laminar flow).

and injection. The fluid in which the ramp vortex is embedded then re-establishes a predominately axial direction of travel over the remaining length of the duct. The drop in circulation in the base region is due to additional vorticity due to injection and base effects. Small oscillations in the circulation near the end of the combustor are believed due to shocks caused by injection and three-dimensional effects. Stokes theorem is obeyed closely by both fine and coarse grid inviscid solutions. The primary difference observed is between the fine and coarse grids in the ramp base region where the coarse grid substantially underpredicts the drop in circulation. However, both coarse and fine grids have similar values of circulation at the end of the near-field region (11 cm).

Figure 7 illustrates the computed flow moment-of-momentum and the computed torque (moments due to pressure forces) for the inviscid ramp cases a and b. Plots of these two quantities are shown for both fine and coarse grids. The torque on the control volume is seen to increase smoothly to the end of the ramp with a slight decline in rate due to three-dimensional relieving effects. The flow in the base region is perturbed between 4–6 cm. The net torque then changes sign at about 9 cm. This is due to the three-dimensional advancing shock structure propagating downstream of the ramp and inducing a progressive imbalance in circumferential wall pressures. The computed torque and the computed moment-of-momentum correspond almost exactly for the fine grid over the ramp length and well into the ramp base region. The slight divergence that begins in this region is believed due to flow unsteadiness. The moment-of-momentum and the torque have become approximately equal at the end of the near-field region (11 cm). Similar trends are observed for the coarse grid case (case b). Overall, computed torque and flow moment-of-momentum are very similar for all inviscid cases shown.

Figure 8 is a plot of the near-field circulation strength for the laminar case c. Both line integral and vorticity integrated methods for computing circulation yield nearly identical results over the length of the ramp, but differ slightly in the midrange (ramp base region). The two quantities have approximately the same value at the end of the elliptic region (11 cm). The influence of the cross-stream counter-rotating vorticity, which is established near the walls due to the no-slip condition, lowers the overall circulation magnitude approximately 33% from the inviscid case. From a fuel mixing standpoint, this decrease is not necessarily significant since the "main" outer vortex can be shown to not be appreciably diminished in strength over the length examined. Downstream (not shown) the circulation oscillates somewhat due to shocks, although a slow damping is observed due to laminar shear diffusion.

The computed torque and flow moment-of-momentum (Fig. 9) for case c (laminar flow) demonstrates that there is a small deviation between the two quantities in the base region (between 4–6 cm). Since both torque and moment-of-momentum are computed with reference to the ramp inflow (i.e., net torque), this deviation persists into the downstream region as shown. The rate of change in torque compares well with the change in flow moment-of-momentum beyond the unsteady base region.

In order to study the impact of downstream turbulence on mixing for these cases, a turbulent case d is analyzed in comparison with the laminar case c. Figure 10 illustrates a comparison of mixing efficiency for these two cases. Here, the

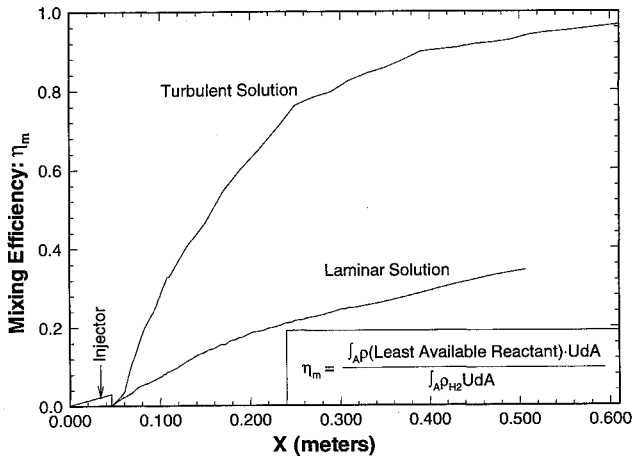


Fig. 10 Mixing efficiency vs $x$ (laminar and turbulent flow).

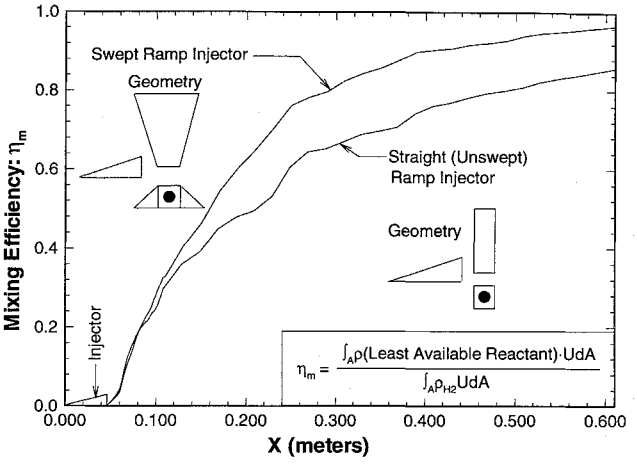


Fig. 11 Mixing efficiency vs $x$ (swept and unswept ramp).

mixing efficiency is defined at each cross-sectional plane as the ratio of the integrated mass flux of the least available reactant if complete reaction takes place (with no further mixing) to the integrated total mass flux of the least available reactant. This describes the degree of mixing of the fuel and the oxidizer and varies between 0–1. The turbulent case has approximately three times the mixing of the laminar case across the length of the combustor, even with the jet-to-free-stream velocity ratio of 1.0 in both cases. Although the turbulent mixing predicted for such complex high enthalpy flows must be viewed cautiously at best (due to the simplicity of the model used), this plot provides an indication of the dominant role of turbulence in actual fuel-air mixing processes, and hence, of the importance of turbulence models in general. The role of the axial vorticity is not entirely clear in Fig. 10; its impact on mixing may or may not be proportionally greater in the turbulent case.

The additional mixing that is obtained by sweeping the sides of the injector ramp is clearly shown in Fig. 11 in which mixing efficiencies are plotted vs axial distance for both an unswept ramp (case e) and the swept ramp (case d). As discussed earlier, the swept ramp has a relatively stronger bow shock that results in a stronger spillage-induced vortex. (The ramp base circulation strength for the unswept ramp is approximately two-thirds of the circulation strength of the swept ramp at the same location.) The vortex generated by the overspill increases the lateral and vertical stretching of the fuel-air interface in the downstream duct such that swept ramp mixing efficiency is approximately 25% greater than the unswept ramp mixing efficiency. The concept of the crossflow movement of the flow and its relationship to the mixing is clarified by defining a $L_{vs}$. The vortex stirring length is the cumulative distance that an average flow particle travels in the crossflow plane as it travels from the ramp base to the combustor exit or

$$L_{vs} = \int \frac{|q_{cross}|}{U_{avg}} \, dx \tag{3}$$

Here, $q_{cross}$ is the magnitude of the crossflow component of the velocity vector, and $U_{avg}$ is the effective axial velocity at a given crossflow plane. Both $q_{cross}$ and $U_{avg}$ are area-averaged on a crossflow plane in this study. This parameter is plotted vs mixing efficiency for the swept and unswept ramp cases in Fig. 12. This figure illustrates a distinct linear relationship between the vortex stirring length and the mixing efficiency (except as expected near the asymptotic approach to a mixing efficiency of 1.0 for both cases). The vortex stirring length as shown here is a very simple physical parameter that demonstrates in a clear and unambiguous fashion the impact of the generated vortex strength on fuel-air mixing in supersonic flow.

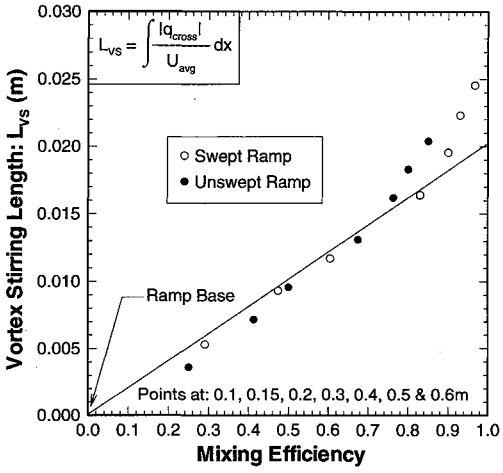


Fig. 12 Vortex stirring length vs mixing efficiency.

The next step in this investigation is to eliminate the influence of the swept ramp vortex in order to examine vortex/nonuniformity influence on downstream mixing. This leads to the definition of two additional cases. Case f is a laminar swept ramp (turbulent in the downstream) with fuel injection from the entire ramp base. The injectant pressure is lowered to match the same fuel equivalence ratio as the previous cases. Case g is a similar case with an identical ramp flowfield upstream, but with the flow suitably one dimensionalized at the ramp base. The one-dimensionalization scheme used here identically conserves all mass, momentum, and energy fluxes.[15] This technique eliminates all nonuniformities at the ramp base including the vortex and the bow shock, both which contribute to downstream mixing. Note that by filling the base with fuel, base effects in these cases are eliminated as well. A comparison of computed mixing efficiency for the two cases f and g (Fig. 13) demonstrates that removing the three dimensionality at the ramp base (injection location) results in a 40% lowering of the overall mixing efficiency in the midrange of the combustor. Curiously, in the near field (out to approximately 10 cm), the mixing is similar for the two cases. At this point, the rate of mixing for the vortex/shock removed case g declines quite rapidly. The vortex apparently inhibits mixing in the very near field of the base in case f. Note that the mixing rate decline in case g begins in the near-field region itself (before $x$ = 10 cm). A comparison of Fig. 10 (case d) and Fig. 13 (case f) also indicates that ramp base injection details do not significantly effect mixing. This implies that marching codes may be successfully used to simulate such flowfields (in which near-field modeling techniques are suitably employed).

The final case h examined in this study is a similar ramp for which experimental data has been obtained in the HY-

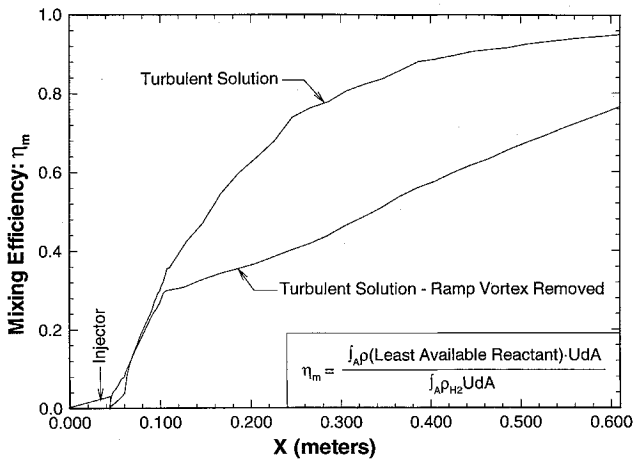


**Fig. 13 Mixing efficiency vs $x$ (with and without ramp vortex).**

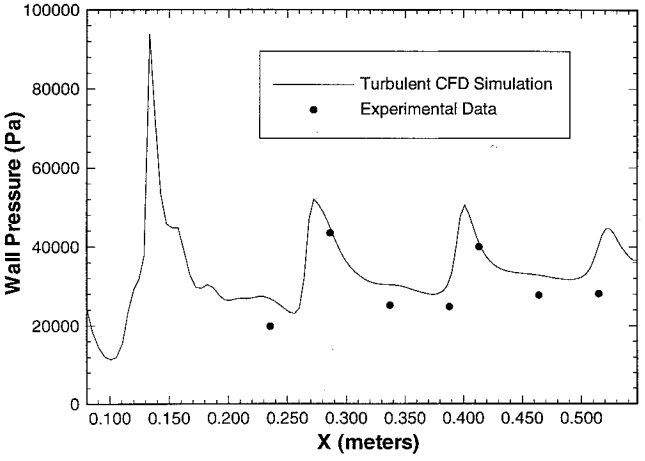


**Fig. 14 Wall pressure (experimental and computational) vs $x$.**

PULSE facility. This ramp is tested at similar flow conditions to those used for computational cases a–g. In these experiments, two side-by-side swept ramp injectors with similar geometries as described for cases a–d were tested. For case h, a viscous side wall and upstream duct section are included in the numerical modeling effort. The injectant is complex, with both water and unburnt hydrogen as well as solid particles (which were needed for flow visualization tests). Note that this was a mixing experiment with nitrogen on the inflow. Overall fuel mixing efficiency at a near-field station (3 in. from the ramp base) as computed from the CFD is in excellent agreement with the experimentally determined value. Figure 14 is a plot of wall pressure on the duct centerline (injector side) vs axial distance measured from the duct leading edge (located approximately 16 cm upstream of the ramp leading edge). This plot shows fair agreement with the data. Discrepancies are believed to be due to the simplified turbulence model used. In addition, the turbulent Prandtl number used here, like the turbulent Schmidt number, has, in fact, a complex spatial distribution that is not accurately represented in the simulation.

## Conclusions

Efficient generation of the vorticity from flush-wall or intrusive injectors is important for fast mixing of fuel and oxidizer in scramjet combustors. This article provides a detailed comparative study of such vorticity from intrusive injector ramps in high enthalpy (flight Mach number of 13.5) scramjet flowfields. In addition, the impact of this vorticity on mixing is discussed. Results from both inviscid and viscous cases are presented in terms of classic circulation. This quantity demonstrates dominant features of the highly complex flows established near and downstream of ramp injectors. Grid refinement performed in this investigation shows that overall circulation (or vortex strength) and its evolution along the combustor can be analyzed with a relatively coarse CFD grid. This study also indicates that crossflow shear in actual viscous (and especially turbulent) flows may cause a lowering in the strength of the vortex shed from the ramp. This is due primarily to the action of the combustor walls in setting up a countervortex. Excellent agreement between the circulation as computed with the area-integrated vorticity and with the circulation as computed using the velocity line integral demonstrates that the CFD solutions are closely obeying Stokes law for both inviscid and viscous cases. In addition, the computed flowfields and associated torques are shown to obey the fundamental fluid dynamic moment-of-momentum theorem. This provides confidence that the engineering simulations are accurately representing the vorticity flowfield.

The dominant role of turbulent mixing in combustor flowfields downstream of injector ramps is clearly demonstrated by comparing mixing efficiencies for laminar and turbulent flows. Furthermore, computed mixing efficiencies for swept and unswept ramp cases illustrate the additional mixing that is obtained by sweeping the ramp sides. This leads to the concept of a $L_{vs}$, which is the cumulative distance that an average fluid particle travels in the crossflow plane as it transits the combustor from the plane of injection to the exit plane. It is uniquely related to the degree of stretching of the fuel-air interface. The vortex stirring length is linearly related to fuel-air mixing and correlates both swept and unswept ramp cases. In order to further investigate the influence of the axial vorticity on mixing, two additional cases are defined. In these cases, the influence of ramp base effects on mixing is eliminated by filling the base with injection. One of these cases computes the downstream flowfield in which the ramp vortex and three dimensionality are "removed" from the flow. A comparison of mixing efficiency for these cases illustrates the large impact that the vortex structure (as well as other nonuniformities) has on mixing. Additionally, the comparison of cases with and without base effects demonstrates that marching techniques (which are much more resource efficient), may be successfully used to simulate ramp injector flowfields.

Finally, a case is presented in which a similar swept-ramp geometry is simulated in a combustor duct corresponding to an actual HYPULSE experiment. A comparison with downstream experimental data (wall pressure) shows fair agreement. More experimental and numerical work is needed in order to successfully quantify the spatial distributions (or a global equivalent as used here) of both the turbulent heat and the turbulent mass diffusion for such flows.

## Acknowledgments

This work was performed under NASA Grant NAG-1189. Particular thanks are due Charles McClinton, Bob Bittner, and Sharon Stack of the National Aero-Space Program Office at NASA LaRC. Clayton Rogers of the Hypersonic Propulsion Branch at NASA LaRC is also thanked for his continual support, advice, and assistance in this and related work.

## References

[1]Riggins, D. W., McClinton, C. R., Rogers, R. C., and Bittner, R. D., "A Comparative Study of Scramjet Injection Strategies for High Mach Number Flows," AIAA Paper 92-3287, July 1992.

[2]Riggins, D. W., Mekkes, G. L., McClinton, C. R., and Drummond, J. P., "A Numerical Study of Mixing Enhancement in a Supersonic Combustor," AIAA Paper 90-0203, Jan. 1990.

[3]Waitz, I., Marble, F., and Zukowski, E., "A Systematic Experimental and Computational Investigation of a Class of Contoured Wall Fuel Injectors," AIAA Paper 92-0625, Jan. 1992.

[4]Povinelli, F. P., Povinelli, L. A., and Hersch, M., "Effect of Angle of Attack and Injection Pressure on Jet Penetration and Spreading from a Delta Wing in Supersonic Flow," NASA TM-X-1889, Sept. 1969.

[5]Hersch, M., and Povinelli, L. A., "Effect of Interacting Vortices on Jet Penetration into a Supersonic Stream," NASA TM-X-2134, Nov. 1970.

[6]Swithenbank, J., Eames, I., Chin, S., Ewan, B., Yang, Z., Cao, J., and Zhao, X., "Turbulence Mixing in Supersonic Combustion Systems," AIAA Paper 89-0260, Jan. 1989.

[7]Drummond, J. P., Carpenter, M. H., and Riggins, D. W., "Mixing and Mixing Enhancement in Supersonic Reacting Flowfields," *High Speed Flight Propulsion Systems*, edited by S. N. B. Murthy and E. T. Curran, Vol. 137, Progress in Astronautics and Aeronautics, AIAA, Washington, DC, 1991, pp. 383–455.

[8]Riggins, D. W., and McClinton, C. R., "A Computational Investigation of Flow Losses in a Supersonic Combustor," AIAA Paper 90-2093, July 1990.

[9]Bobskill, G., Bittner, R., Riggins, D. W., and McClinton, C. R., "CFD Evaluation of Mach 17 HYPULSE Scramjet Combustor Data," AIAA Paper 91-5093, Dec. 1991.

[10]Bakos, R. J., Tamango, J., Rizkalla, O., Pulsonetti, M. V., Chinitz, W., and Erdos, J. I., "Hypersonic Mixing and Combustion Studies in the GASL HYPULSE Facility," AIAA Paper 90-2095, July 1990.

[11]Drummond, J. P., Rogers, R. C., and Hussaini, M. Y., "A Detailed Numerical Model of a Supersonic Reacting Mixing Layer," AIAA Paper 86-1427, June 1986.

[12]Carpenter, M. H., "Three-Dimensional Computations of Cross-Flow Injection and Combustion in a Supersonic Flow," AIAA Paper 89-1870, June 1989.

[13]Kamath, H., "Parabolized Navier-Stokes Algorithm for Chemically Reacting Flows," AIAA Paper 89-0386, Jan. 1989.

[14]McClinton, C. R., "CFD Support of NASP Design," AIAA Paper 90-3252, Sept. 1990.

[15]Riggins, D. W., and McClinton, C. R., "Analysis of Losses in Supersonic Mixing and Reacting Flows," AIAA Paper 91-2266, July 1991.